Production of Strange Secondaries in High Energy $\Sigma^- A$ Collisions

G.H. Arakelyan*, A.B. Kaidalov**, C. Merino***, and Yu.M. Shabelski****

* Yerevan Physics Institute
Armenia E-mail: argev@mail.yerphi.am

** Institute of Theoretical and Experimental Physics
Moscow, Russia
E-mail: kaidalov@itep.ru

*** Departamento de Física de Partículas and
Instituto Galego de Física de Altas Enerxías
Universidade de Santiago de Compostela
Galiza, Spain
E-mail: merino@fpaxp1.usc.es

**** Petersburg Nuclear Physics Institute
Russia
E-mail: shabelsk@thd.pnpi.spb.ru

Abstract

We describe the WA89 Collaboration experimental data on Λ, Σ^-, Σ^+, Ξ^-, and Ω^- baryons, and $\bar{\Lambda}$ and $\overline{\Xi}^+$ antibaryons production in Σ^- collisions with C and Cu targets at 345 GeV/c ($\sqrt{s_{\Sigma N}} \approx 25.5$ GeV) in the frame of the Quark-Gluon String Model. How the theoretical results compare to the experimental data is discussed. Finally, some relations among the values of the model parameters obtained with the help of quark combinatorics are presented.

PACS. 25.75.Dw Particle and resonance production

1 Introduction

The Quark-Gluon String Model (QGSM) and the Dual Parton Model (DPM) are based on the Dual Topological Unitarization (DTU) and they quantitatively describe [1-6] many features of high energy production processes, including the inclusive spectra of different secondary hadrons, their multiplicities and multiplicity distributions, etc., both in hadron-nucleon and hadron-nucleus collisions at fixed target energies. QGSM and DPM account for the main features of secondary production at collider energies.

In the QGSM, high energy interactions are considered as proceeding via the exchange of one or several Pomerons, and all elastic and inelastic processes result from cutting through or between Pomerons [7]. Each cut Pomeron leads to the production of two strings of secondaries. The inclusive spectra of hadrons in the final state of the collision are related to the corresponding fragmentation functions of the quarks and diquarks at the end of the strings. These fragmentation functions are constructed by using the Reggeon counting rules [9].

To study the interaction with a nuclear target the Multiple Scattering Theory (Gribov-Glauber Theory) is used, and, thus, this interaction is considered as the superposition of the interactions of the incident hadron with different nucleons in the target [5, 8].

In previous papers [1-6], where the secondary production by proton, pion, and kaon beams was reasonably described, the model parameters were already fixed by comparison of the theoretical calculations with experimental data.

Here we consider the production of secondaries in $\Sigma^- C$ and $\Sigma^- Cu$ collisions and we present the comparison of the theoretical results with the experimental data at 345 GeV/c obtained by the WA89 Collaboration [10]. To include in our description interactions out of Σ^- beams we have to deduce the expressions both of the momentum distribution function of ds diquark in Σ^- hyperon, and of its fragmentation functions into secondary hadrons.

However, in the case of Σ^- beam the agreement with the experimental data of the calculations obtained by using these standard fragmentation functions is not good enough. The agreement becomes better when some additional polynomial factors are included into our fragmentation functions, but it is not clear whether this is a result of some special structure of the strange baryons and their resonances, or it is simply connected to possible experimental inconsistencies.

2 Production of secondaries on nuclear targets in QGSM

In QCD hadrons are composite bound state configurations built up from the quark $\psi_i(x), i = 1, ...N_c$, and gluon $G^\mu_a(x), a = 1, ..., N_c^2 - 1$, fields. In string models baryons are considered as configurations consisting of three strings attached to three valence quarks and connected at one point (small volume) x, called the "string junction" (SJ) [11-13].

The corresponding wave function can be written as

$$\begin{aligned} |B\rangle &= \psi_i(x_1)\cdot\psi_j(x_2)\cdot\psi_k(x_3)\cdot J^{ijk}(x,x_1,x_2,x_3)\ , \\ J^{ijk}(x,x_1,x_2,x_3) &= \Phi^i_{i'}(x_1,x)\cdot\Phi^j_{j'}(x_2,x)\cdot\Phi^k_{k'}(x_3,x)\cdot\epsilon^{i'j'k'}\ . \end{aligned} \tag{1}$$

Here the operator $\Phi^i_{i'}(x_1,x)$ represents the gluon field string with endpoints at x_1 and x. Such a "star" (or Y configuration of the baryon wave function $|B\rangle$ is favoured [11, 13] with respect to the also possible "triangle" (or Δ) configuration.

Let us discuss in more detail the processes in which one or several Pomerons are exchanged. Each exchanged Pomeron in hadron-nucleon and hadron-nucleus interaction corresponds to a cylindrical diagram that, when cut, produces two showers of secondaries. The inclusive spectrum of secondaries is determined by the convolution of diquark, valence quark, and sea quark distributions, $u(x,n)$, in the incident particles with the fragmentation functions, $G(z)$, of quarks and diquarks into the different hadrons. The diquark and quark distribution functions depend on the number of cut Pomerons, n, in the considered diagram.

In the QGSM one calculates the invariant cross section

$$\frac{x_E}{\sigma_{inel}}\cdot\frac{d\sigma}{dx} = \int\frac{E}{\sigma_{inel}}\cdot\frac{d\sigma}{d^3p}\cdot d^2p_T\ , \tag{2}$$

where $x=2p_\parallel/\sqrt{s}$ is the Feynman variable x_F, and $x_E=2E/\sqrt{s}$, and one has then to use one value of $\langle p_T^2\rangle$ (here we have taken the value $\langle p_T^2\rangle = 0.35$ (GeV/c)^2) to make the transition to the values of $d\sigma/dx_F$ which are presented in the experimental papers [10].

Thus, for the case of a nucleon target the inclusive spectrum of a secondary hadron h in QGSM has the form [1]:

$$\frac{x_E}{\sigma_{inel}}\cdot\frac{d\sigma}{dx} = \sum_{n=1}^{\infty} w_n\cdot\phi^h(x,n) + w_D\cdot\phi^h_D(x)\ . \tag{3}$$

The functions $\phi^h(x,n)$ determine the contribution of diagrams with n cut Pomerons, and w_n is the probability for this process with n cut Pomerons to occur [15]. The second term in the right-hand side of Eq. (3) describes the contribution of diffraction dissociation processes, where the triple-Reggeon diagrams are also included [1, 3]. The expressions of $\phi^h(x,n)$ for ΣN ($N=p,n$) collisions in Eq. (3) have the form [1, 14]:

$$\phi^h_{\Sigma N}(x,n) = f^h_{qq}(x_+,n)\cdot f^h_q(x_-,n) + f^h_q(x_+,n)\cdot f^h_{qq}(x_-,n) + 2(n-1) f^h_s(x_+,n)\cdot f^h_s(x_-,n)\ , \tag{4}$$

where

$$x_\pm = \frac{1}{2}[\sqrt{4m_T^2/s + x^2}\pm x]\ , \tag{5}$$

with $m_T=\sqrt{m^2+p_T^2}$ the transverse mass of the produced hadron, and f_{qq}, f_q, and f_s corresponding to the contributions of diquarks, valence quarks, and sea quarks, respectively. The quantities $f_i(x_+,n)$ and $f_i(x_-,n)$ account for the contributions to $\phi(x,n)$ of the Σ-hyperon beam and of the target nucleon, and they are determined by the convolution

of the diquark and quark distribution functions with the corresponding fragmentation functions, e.g.,

$$f^h_{qq}(x_+, n) = \int_{x_+}^1 u_{qq}(x_1, n) \cdot G^h_{qq}(x_+/x_1)\ dx_1. \tag{6}$$

For the case of nuclear targets one has to consider the different possibilities of one or several Pomeron cuts in each of the ν hadron-nucleon inelastic interaction blobs, as well as of cuts between Pomerons. For a $\Sigma^- A$ collision, one of the cut Pomerons links a valence diquark and a valence quark of the hyperon projectile with a valence quark and a diquark of one target nucleon, respectively, while the additional Pomerons link the sea quark-antiquark pairs of the projectile, either with diquarks and valence quarks, or with sea quark-antiquark pairs, of the target nucleons.

As one example, the diagram for the inelastic interaction of the Σ^--beam with two target nucleons is shown in Fig. 1. In the blob of the $\Sigma^- N_1$ inelastic interaction one Pomeron is cut, while in the blob of the $\Sigma^- N_2$ interaction two Pomerons are cut. To include all diagrams, i.e. to account for all possible Pomeron configurations and permutations, is essential for a correct calculation. The process shown in Fig. 1 satisfies the condition that the absorptive part of the hadron-nucleus amplitude is determined by combinations of the absorptive parts of hadron-nucleon interactions, according to rules given in refs. [16-19].

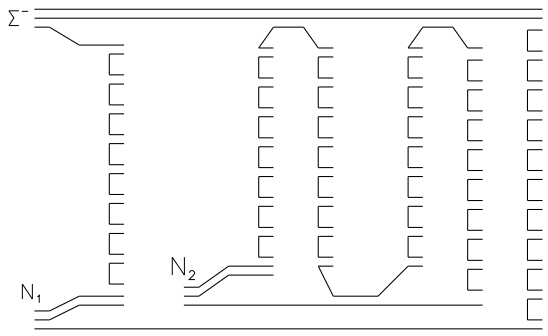

Figure 1: One of the diagrams for the inelastic interaction of an incident Σ^--hyperon with two target nucleons N_1 and N_2 in a $\Sigma^- A$ collision.

For hA collisions, where n inelastic interactions occur with ν target nucleons, one has that $n \geq \nu$, and $1 \leq n_i \leq n - \nu + 1$, n_i being the number of cut Pomerons connecting with the i-th target nucleon. By denoting the relative weight of the contribution with n_i cut Pomerons in every hN blob as $w^{hN}_{n_i}$, and by using the same procedure as in ref. [5], we can write the corresponding expressions for the inclusive spectrum of the secondary hadron h produced in a ΣA collision, where all possible Pomeron permutations and all possible different quark contents of the protons and neutrons in the target have to be accounted for.

In particular, the contribution to the inclusive spectrum of the diagram in Fig. 1 is written as follows:

$$\frac{x_E}{\Sigma_{\Sigma A}^{prod}} \cdot \frac{d\sigma}{dx_F} = 2V_{\Sigma A}^{(2)} \cdot w_1^{\Sigma N_1} \cdot w_2^{\Sigma N_2} \cdot \Big\{ f_{qq}^h(x_+,3) \cdot f_q^h(x_-,1) + f_q^h(x_+,3) \cdot f_{qq}^h(x_-,1) + f_s^h(x_+,3) \cdot [f_{qq}^h(x_-,2) + f_q^h(x_-,2) + 2f_s^h(x_-,2)] \Big\} \ , \quad (7)$$

where $V_{\Sigma A}^{(\nu)}$ is the probability of pure inelastic (non diffractive) interactions with ν target nucleons of a nucleus A to occur.

The diquark and quark distributions, as well as the fragmentation functions, are determined from Regge intercepts, and their expressions were presented in Appendix 1 of ref. [20] (see also [21, 22]). Now, for the case of the presence of a ds diquark in the beam, they are given in the Appendix of this paper (see below).

For secondary baryon production, the diquark fragmentation function contains two contributions. The first one corresponds to the production from the sea of a $B\bar{B}$ pair in the midrapidity region (see Fig. 2), and it will be discussed in detail in the Appendix.

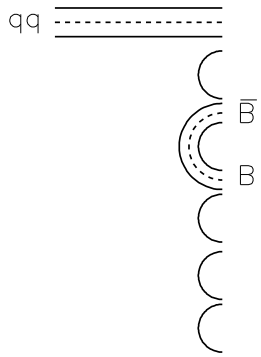

Figure 2: Cut-chain diagram corresponding to the diquark fragmentation function for the production of a central $\bar{B}B$ pair.

The second contribution is connected with the direct fragmentation of the incident diquark into a secondary baryon with conservation of the SJ. In the frame of QGSM three possibilities exist for this second contribution [20]. The secondary baryon can consist of: (a) the SJ together with two valence and one sea quarks, (b) the SJ together with one valence and two sea quarks, and (c) the SJ together with three sea quarks. These three possibilities are shown in Fig. 3.

The fraction of the energy of the incident baryon carried by the secondary baryon decreases from (a) to (c), whereas the mean rapidity gap between the incident and secondary baryon increases.

The processes shown in Figs. 3a and 3b are the standard ones in QGSM and DPM, and they determine the main contribution to the multiplicity of secondary baryons in the fragmentation region.

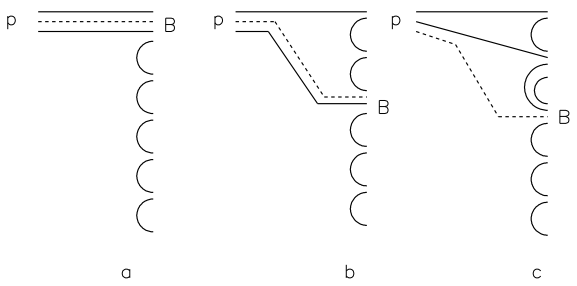

Figure 3: QGSM diagrams describing secondary baryon B production by diquark d: (a) initial SJ together with two valence quarks and one sea quark, (b) SJ together with one valence quark and two sea quarks, and (c) SJ together with three sea quarks.

On the other hand, the diagram shown in Fig. 3c leads to the difference in baryon and antibaryon production at rapidities far from the incident baryon (baryon charge diffusion in rapidity space). The role of such a process in the description of experimental data was considered in detail in refs. [21-26]. For ΣA collisions at 345 GeV/c the relative contribution of this diagram is rather small.

The fragmentation function of diquark d, with quark content $d = q_1 q_2$, into a secondary baryon B through the processes shown in Fig. 3a, 3b, and 3c has the form [20]:

$$G^B_{SJ}(z) = a_N \cdot z^\beta \cdot [v^B_{q_1 q_2} \cdot z^{2.5-\beta} + (v^B_{q_1} + v^B_{q_2}) \cdot z^{2-\beta} \cdot (1-z) + v^B_0 \cdot \varepsilon \cdot (1-z)^2] \cdot (1-z)^\gamma \ . \quad (8)$$

Here $\beta = 1 - \alpha_{SJ}$, with α_{SJ} being the intercept of SJ Regge trajectory, ε is the relative suppression factor of the (c) contribution with respect to the processes (a) and (b), and a_B is a normalization parameter. In the present calculations we use the values $\varepsilon = 0.024$, $\alpha_{SJ} = 0.9$, and $a_N = 1.33$, as in ref. [21]. The factor $(1-z)^\gamma$ accounts for the fact that the intercept of the ϕ-meson Regge trajectory, $\alpha_\phi \approx 0$, is smaller than the standard non-vacuum Reggeon intercept, $\alpha_R \approx 0.5$. The value of the parameter γ is half the difference between the strangenesses of the considered diquark and that of the secondary baryon. The powers of z and $(1-z)$ are changed when either q_1 or q_2 is a strange quark. The values of v^B_i for different quarks i and baryons B are determined by quark combinatorics [26, 27]. These values are presented in the Appendix (see below).

3 QGSM description of the experimental data

The experimental data for Λ, Σ^-, Σ^+, Ξ^-, and Ω^- baryons, $\bar{\Lambda}$ and $\overline{\Xi}^+$ antibaryons production in Σ^- collisions with C and Cu targets are presented in ref. [10] in terms of $d\sigma/dx_F$.

Let us start our analysis from the left panel of Fig. 4, where the data on p spectra at pp collisions and their comparison with our old QGSM calculations are shown. The agreement is good, as it was usually obtained in our previous papers.

For comparison, we also present similar predictions for the case $\Sigma^- p \to \Sigma^- X$, which is theoretically similar to $pp \to pX$, but about 2 times smaller in the region of moderate

x_F. It's generally accepted that this difference can be connected to the rather large probability to produce a Λ in the Σ^- case. At small x_F one also has suppression of the Σ^- production by sea quarks, what leads to a larger difference in the two considered reactions.

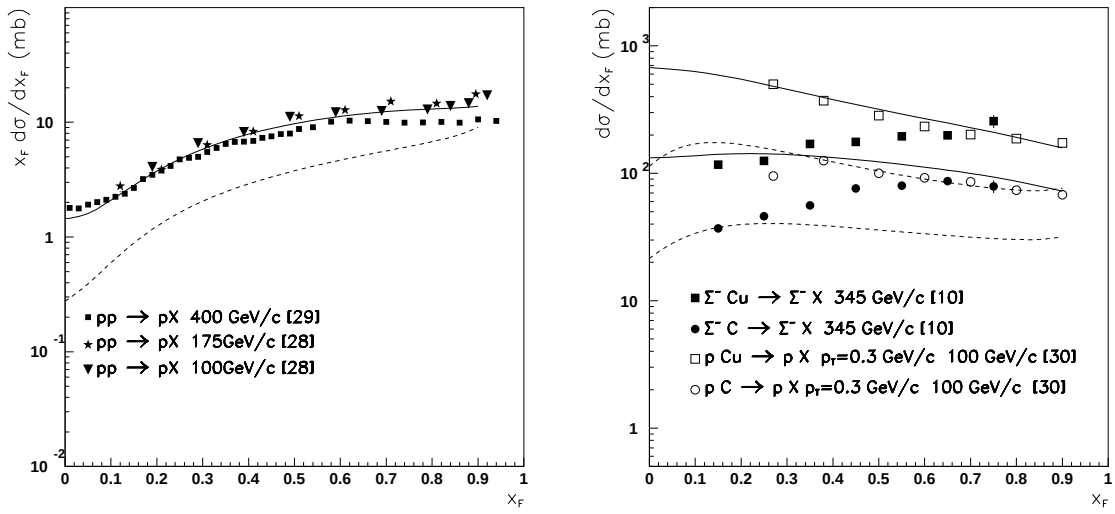

Figure 4: Experimental Feynman-x distributions of secondary p produced in pp collisions at 100, 175, and 400 GeV/c, together with their description by QGSM, and the QGSM predictions for $\Sigma^- p \to \Sigma^- X$ (dashed curve), left panel. Experimental Feynman-x distributions of secondary Σ^- produced in $\Sigma^- C$ and $\Sigma^- Cu$ interactions at 345 GeV/c [10], and similar distributions of secondary p on the same targets [30], and their comparison with the the predictions for Σ^-'s (solid curves) and for protons (dashed curves) by QGSM, right panel.

The experimental data on secondary protons production on nuclear targets at 100 GeV/c and $p_T = 0.3$GeV/c [30] are also in good agreement with the QGSM, as it is shown in right panel of Fig. 4 and in [5]. On the contrary, experimental data for Σ^- production on C and Cu targets shown in the right panel of Fig. 4 are in contradiction with our calculations when we use the fragmentation functions directly taken from the Reggeon counting rules, as it was done in all previous papers [1, 2, 5, 6]. One can immediately see that these data have different shape that the proton data for the same targets. Unfortunately, the proton data [30] presented here were measured at fixed $p_T = 0.3$GeV/c, and there are no proton production data on nuclear targets integrated over p_T, which could be used for direct comparison. However, the difference in the shapes of the distributions seems to be too large, especially when keeping in mind that the data of [30] were successfully described by the QGSM in ref. [5].

Now, let us compare the spectra of secondary Σ^- and Λ obtained in ref. [10]. The calculated ratio of these spectra, together with the corresponding experimental points obtained by using the data of ref. [10], are presented in Fig. 5. Both Σ^- and Λ should be produced in the interval $x_F = 0.3$-0.8 mainly by the process shown in Fig. 3a, when

the ds diquark fragments into them by picking up, either an u or a d-quark from the sea, respectively. The fragmentation functions for both channels should be somehow similar, with differences coming from other contributions including triple-Reggeon terms. This comes from the fact that ds and dd diquarks appear in the incident Σ^- with probabilities 2/3 and 1/3, respectively, and, on top of that, the fragmentation of the dd diquark into strange secondary baryons is suppressed by the strangeness suppression factor S/L (see Appendix). So, the ratio Σ^-/Λ should be approximately constant in the considered interval. However, the experimental ratio of Σ^-/Λ yields increases more than 3 times in the interval $x_F = 0.3$-0.6, in total disagreement with our theoretical expectation. We want to stress that we have never met such a large disagreement with the experimental data in any of our previous calculations, and one has also to note that this disagreement with the experimental data on the ratio Σ^-/Λ can not be corrected by any theoretically meaningful modification of the ds-diquark fragmentation functions.

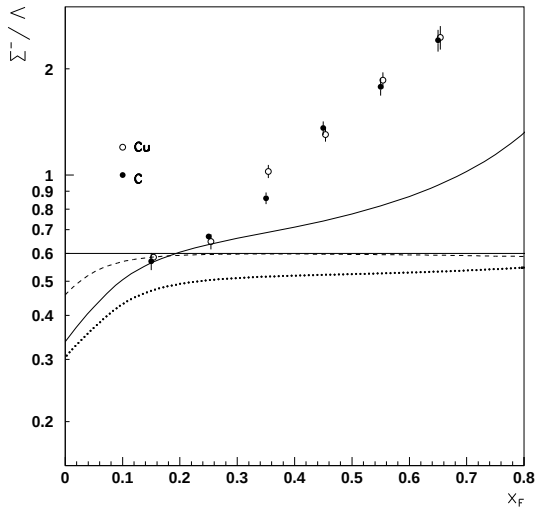

Figure 5: Experimental ratios of secondary Σ^- to Λ yields vs x_F in $\Sigma^- C$ and $\Sigma^- Cu$ interactions at 345 GeV/c [10], together with the QGSM predictions for these ratio (solid curve). The dashed and dotted curves show the ratios when taking into account different contributions to the QGSM calculations (see details in the main text).

The absolute value of Σ^- to Λ ratio in the QGSM is more model dependent. In the simplest approximation, when all final dds states are assumed to be Σ^- and all uds states are assumed to be Λ (secondary Σ^0 are usually registered as Λ after radiative $\Sigma^0 \to \Lambda\gamma$ decay), the ratio Σ^-/Λ is equal to 1. However, this can be changed by the resonance production, e.g. the state $\Sigma^*(1385)$, that can be produced with rather large cross section, has a dominant decay mode $\Lambda\pi$ that would transfer some part of dds states into additional Λ's, and it would thus decrease the Σ^-/Λ ratio.

To account for this effect we assume that when only ds diquark fragmentation is considered, the hyperon production leads to the following empirical rule for the Σ^-/Λ

ratio [27]: fragmentation is considered, the Σ^-/Λ ratio would be.

$$R^{(ds)}_{\Sigma^-/\Lambda} = \Sigma^-/\Lambda = 0.6\ . \tag{9}$$

Such an assumption has provided a reasonable description of the Λ x_F spectra in pp, $p\pi$, kp collisions [20, 21, 22]. Both Σ^- and Λ spectra should be affected by nuclear effects in a similar way.

To show the structure of our calculations in more detail, in Fig. 5 we present the ratio of Σ^- to Λ when only part of all contributions is accounted for. The dashed curve shows the result of calculations when only the first term in the right-hand side of Eq. (4) is considered. In this case the ratio of Σ^- to Λ in the fragmentation region ($x_F \geq 0.2$) is very close to 0.6, the very small difference from this value coming from the contribution of dd diquark fragmentation. At small x_F, the values of x_- in Eq. (5) increase, leading to the decrease of the functions $f^n_q(x_-, n)$ in Eq. (4), and to the decrease of the Σ^-/Λ ratio.

The ratio of Σ^- to Λ production when only fragmentation of ds diquark is considered, and without diffraction dissociation nor triple-Reggeon contributions, is shown in Fig. 5 by a dashed curve. If all diquark and quark terms in Eq. (4) are included (dotted curve), the ratio is smaller and the agreement with the experimental data becomes worse, indicating that the ds diquark is responsible for the value 0.6 of the Σ^- to Λ production ratio. The solid curve shows the result of the complete QGSM calculation with diffraction dissociation and triple-Reggeon contributions, and though now the theoretical curve goes up at large x_F, it still presents a very significant disagreement with the experimental data. It seems clear that the agreement of the QGSM predictions with the experimental data can not be obtained by simply considering a slight variation of any of the contributions in Eq. (4).

As the QGSM can not reproduce the experimental ratio of Σ^- to Λ production, it can not describe separately the x_F-distributions of both Σ^- and Λ, that present clearly different experimental behaviours. It is nevertheless interesting to find out which one, Σ^- or Λ distributions, or both, are at the origine of the disagreement in the ratio. The two x_F distributions for Σ^- and Λ are presented in Fig. 6.

The difference between the Σ^- and the Λ x_F distributions could be explained by assuming that in the case of Λ production, but not in that of Σ^- production, the resonance decay contribution is quite significant. In all cases, when including the resonance decay contribution for Σ^- production the x_F distribution would become softer, i.e. narrower, and consequently the agreement with the experimental data would be worse.

The quark and diquark distribution and fragmentation functions are given by the Reggeon counting rules. Thus, for some fragmentation function $G^h_{qq}(z)$ in Eq. (6) having asymptotical behaviours $G^h_{qq}(z \to 0) \sim z^\alpha$ and $G^h_{qq}(z \to 1) \sim (1-z)^\beta$, the fragmentation function is written as the simplest interpolation of these two asymptotical behaviours in the form [9]:

$$G^h_{qq}(z) = a_h \cdot z^\alpha \cdot (1-z)^\beta\ , \tag{10}$$

where a_h is a parameter which determines the inclusive density of a produced hadron h. We will call such a form of the fragmentation function as the standard one. However, a

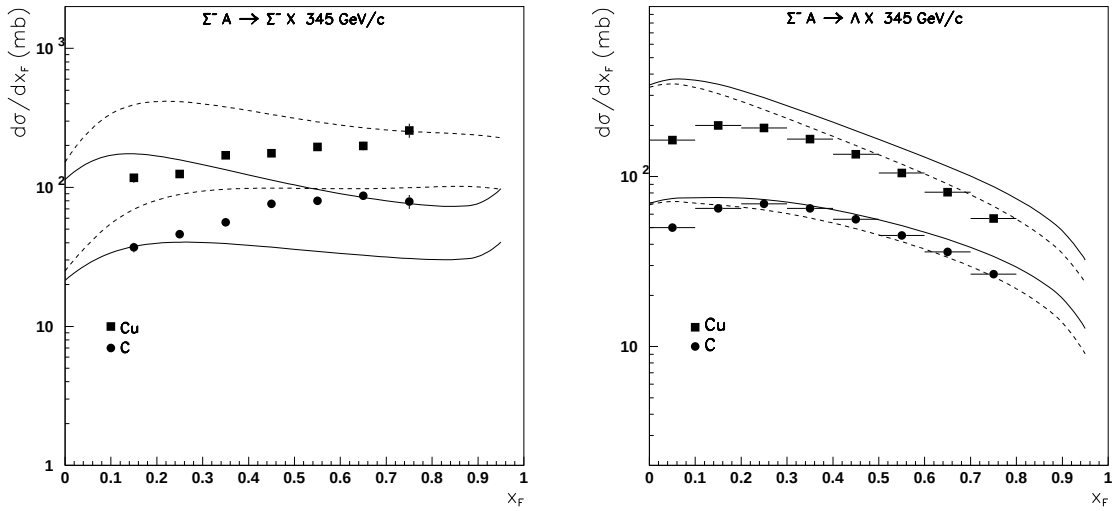

Figure 6: Experimental x_F distributions of secondary Σ^-'s (left panel) and Λ's (right panel), produced in $\Sigma^- C$ and $\Sigma^- Cu$ interactions at 345 GeV/c [10], together with the corresponding QGSM predictions. The solid curves show the result of the calculations with only the standard polynomial terms. The dashed curves in the left panel show the calculations with one additional polynomial factor in the third term of the ds fragmentation function, and the dashed curves in the right panel show the result of the calculations when accounting for the resonance contribution to the spectra of Λ.

slightly more complicate form with additional polynomial factors and new parameters b and b_n is also possible:

$$G^h_{qq}(z) = a_h \cdot z^\alpha \cdot (1-z)^\beta \cdot (1 + b \cdot z^{b_n}) \, . \tag{11}$$

The theoretical x_F distributions of Σ^- and Λ shown by solid curves in Fig. 6 have been calculated by using the standard form of the QGSM fragmentation funactions, without any additional polynomial factor in Eq. (11). The distributions so obtained are in an evident disagreement with the data for the case Σ^- production, and the attempt to include an additional polynomial factor in the fragmentation function of ds diquark (dashed curves in the left panel of Fig. 6) does not lead to any significant improvement of the agreement with the data, since though the absolute values of the spectra increase the shapes remain being wrong.

In the case of Λ production (right panels of Fig. 6), the agreement with the experimental data of the QGSM calculation with the standard form of the fragmentation functions with the experimental data is reasonable, and it becomes better when taking into account that some part of the Λ-hyperons are produced after resonance decay and they consequently have smaller x_F. To include this effect in our calculation we have introduced into the fragmentation function Eq. (A.31)) the additional factor $(1 - \frac{z}{3})$. The QGSM results obtained with this modified fragmenation functions are shown in Fig. 6 by dashed curves.

The spectra of secondary Σ^+ and Ξ^- are shown on Fig. 7. These secondaries are produced with cross sections several times smaller than secondary Σ^- and Λ.

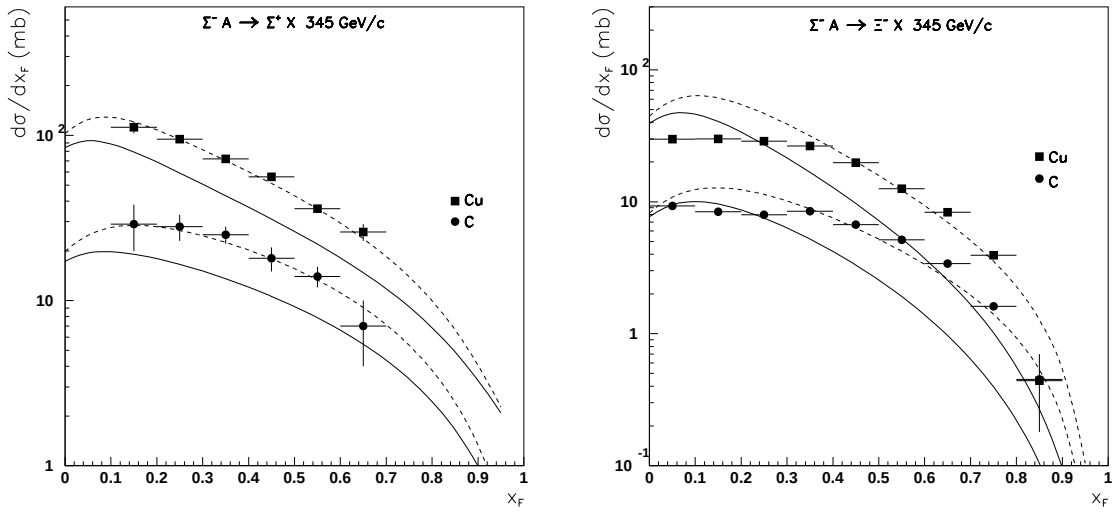

Figure 7: Experimental x_F distributions of secondary Σ^+ (left panel) and Ξ^- (right panel), produced in $\Sigma^- C$ and in $\Sigma^- Cu$ interactions at 345 GeV/c [10], together with the corresponding QGSM predictions. The solid curves show the result of the calculations with only the standard QGSM expressions. The dashed curves are obtained with with one additional polynomial factor in the fragmentation functions.

In the standard approximation of the QGSM, for Σ^+ production only one valence s quark, Eq. (A.14), as well as an s quark through the diagram in Fig 3b, from the incident Σ^- can be used to fragment into Σ^+, but another possibility that is usually considered is the resonance production of $\Sigma^{*0}(1385)$ or $\Lambda(1405)$ in the process of ds-diquark fragmentation (see Fig. 3a), and the subsequent decay into $\Sigma^+\pi^-$. The results of the calculations in this approximation (shown by solid curves in the left panel of Fig. 7) are in reasonable agreement with the experimental data. The shapes of the curves are correct, though the normalization are underestimated on the level of 30%. This disagreement can be corrected (dashed curves in the left panel of Fig. 7) by introducing a polinomial factor $(1+5\cdot z)$ into the last term of the ds diquark fragmentation function in Eq. (A.35).

For the case of Ξ^- production (right panel of Fig. 7) the contribution of the ds-diquark fragmentation is decreased by the strangeness production suppression factor. The calculation of Ξ^- production with only the standard terms in the diquark fragmentation functions (solid curves in the right panel of Fig. 7) results in a too fast decrease of the spectra when increasing x_F. The calculation with an additional polinomial factor $(1+3\sqrt{z})$ in the last term of the diquark fragmentation function Eq. (A.38) leads to a better agreement with the experimental data (dashed curves on the right panel of Fig. 7), except for the region of low x_F, where the model results are significantly higher than the experimental data.

In the case of secondary Ω^- production by Σ^- beam, the incident s quark should pick up two strange quarks from the sea. The cross section of this process should clearly be small due to the presence of the squared strangeness suppression factor. The experimental points for secondary Ω^- production are presented in Fig. 8. Here the standard QGSM predictions are in reasonable agreement with the data.

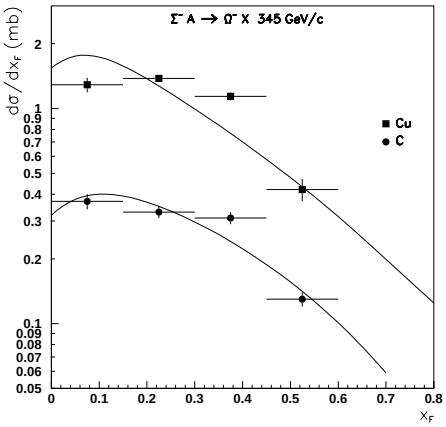

Figure 8: The x_F distributions of secondary Ω^-'s produced in $\Sigma^- C$ and $\Sigma^- Cu$ interactions at 345 GeV/c [10]. The curves show the QGSM predictions with only the standard QGSM expressions in the diquark fragmentation functions.

The experimental yields of $\bar{\Lambda}$'s and $\overline{\Xi}^+$'s [10], which only contain sea antiquarks and do not depend on the SJ contribution, are shown in Fig. 9. The corresponding description by the standard QGSM fragmentation functions clearly underestimates the $\bar{\Lambda}$ yields at $x_F > 0.4$. For the case of $\overline{\Xi}^+$ production the agreement is reasonable. The description of the $\bar{\Lambda}$ and $\overline{\Xi}^+$ spectra obtained by using the fragmentation functions of eqs. (A.20) and (A.21), where an additional polinomial factor $(1 + 20 \cdot z^2)$ has been included, leads to a better agreement with the experimental data of the $\bar{\Lambda}$ spectra, letting apart some overestimation in the small x_F region.

4 Conclusions

We present the QGSM description of the experimental data [10] on secondary hyperon production in $\Sigma^- C$ and $\Sigma^- Cu$ collisions at 345 GeV/c. These data are of special interest because the main contribution to the spectra of secondary Λ, Σ^-, and Ξ^- at $x_F \geq 0.3$ comes from the direct fragmentation Fig. 3a of the incident ds diquark, with rather small background from another subprocesses.

From the invariant cross section in Eq. (3) and by using the value $\langle p_T^2 \rangle = 0.35$ $(\mathrm{GeV/c})^2$, we get the values of $d\sigma/dx_F$ that could be compared to those presented in the experimental papers [10]. In all cases, except for Σ^+ production, we overestimate the experimental data at small x_F.

In the region $x_F > 0.3$-0.4, practically all the experimental x_F distributions measured by the WA89 Collaboration [10] are wider than the corresponding QGSM predictions ob-

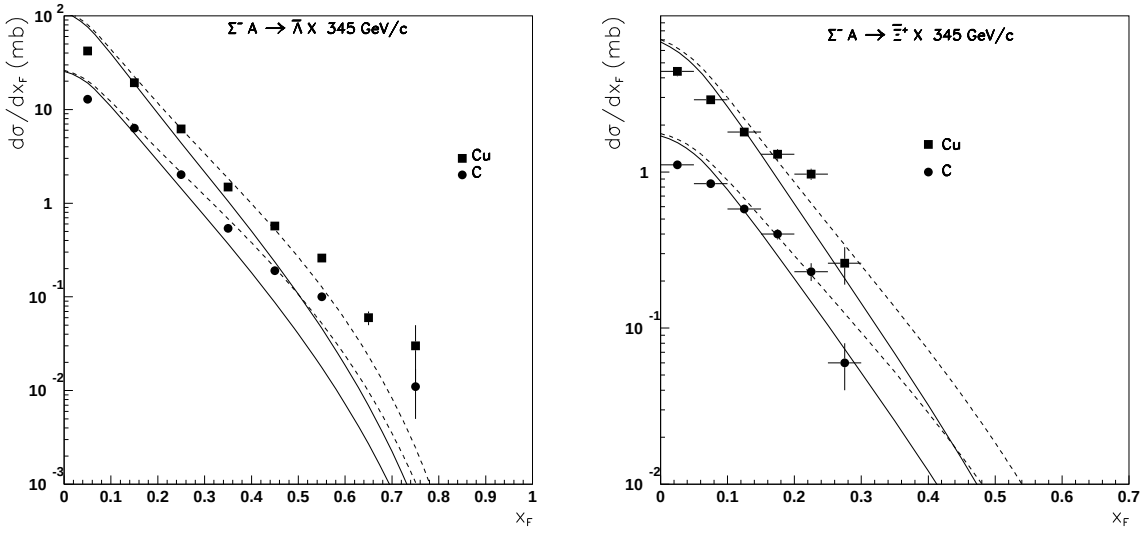

Figure 9: The x_F distributions of secondary $\bar{\Lambda}$ (left panel) and $\bar{\Xi}^-$ (right panel) produced in $\Sigma^- C$ and in $\Sigma^- Cu$ interactions at 345 GeV/c, together with the corresponding standard QGSM calculations (solid curves) and with the QGSM calculations obtained by including an additional polynomial factor into the ds fragmentation functions of eqs. (A.20) and (A.21).

tained by using the standard diquark fragmentation functions given by Reggeon counting rules. To solve this steady disagreement, we have included in the diquark fragmentation functions (mainly in ds diquark fragmentation) one additional polynomial factor which takes the spectra up at $x_F > 0.3$-0.4. Another problem faced when trying to describe the experimental data of ref. [10] is connected with the behaviour at small x_F. The peaks present in the theoretical estimations and shown in Fig. 8 are the natural result of dividing the rather flat function $x_E \cdot \frac{d\sigma}{dx}$ by x_E. The experimental behaviours of $d\sigma/dx$ correspond, on the contrary, to deep minima in $x_E \cdot \frac{d\sigma}{dx}$.

Nevertheless, the most disturbing question we face when comparing the QGSM predictions for the x_F spectra of secondary hyperons comes from the fact that the experimental x_F distributions of secondary Σ^- are very different to the corresponding x_F spectra of secondary protons in pA collisions. Since the standard QGSM predictions have always provided a good agreement with the experimental data on the x_F spectra of secondary non-strange secondaries, from the theoretical point of view it would be puzzling if the disagreement of the corresponding spectra of strange secondaries with the experimental data would be confirmed. On top of that, should the theoretical predictions for the Σ^- case be modified to agree with the currently available experimental data, this would mean significant changes in the standard QGSM diquark distributions and/or in the ds-diquark fragmentation function to Σ^-. However, one actually has not any apparent theoretical support for those changes, and that could even result in the violation of the SU(3) flavour symmetry. Let's then see whether the experimental data on the x_F spectra for secondary Σ^- will be confirmed or corrected in the future.

Acknowledgements

This paper was supported by Ministerio Educación y Ciencia of Spain under the Spanish Consolider-Ingenio 2010 Programme CPAN (CSD2007-00042), by Xunta de Galicia (Galiza, Spain) under project FPA2008-01177, and also by Universidade de Santiago de Compostela through grants RFBR-07-02-00023 and RSGSS-1124.2003.2.

Appendix

The diquark and quark distribution functions in Σ^--baryon for a diagram with n cut Pomerons have been parametrized as follows:

$$u_{dd}(x,n) = C_{dd}\cdot x^{\alpha_R-2\alpha_B}\cdot(1-x)^{-\alpha_\varphi+m_2}\ , \tag{A.1}$$
$$u_{ds}(x,n) = C_{ds}\cdot x^{\alpha_R-2\alpha_B+(\alpha_R(0)-\alpha_\varphi(0))}\cdot(1-x)^{-\alpha_R+m_1}\ , \tag{A.2}$$
$$u_{d}(x,n) = C_{d}\cdot x^{-\alpha_R}\cdot(1-x)^{\alpha_R-2\alpha_B+(\alpha_R(0)-\alpha_\varphi(0))+m_1}\ , \tag{A.3}$$
$$u_{s}(x,n) = C_{s}\cdot x^{-\alpha_\varphi}\cdot(1-x)^{\alpha_R-2\alpha_B+m_2}\ , \tag{A.4}$$
$$u_{sea}(x,n) = C_{s}\cdot x^{-\alpha_R}\cdot(1-x)^{\alpha_R-2\alpha_B+n-1+k}\ . \tag{A.5}$$

The values of m_1 and m_2 in Eqs. (A.1)-(A.4) are determined from momentum conservation:

$$\langle x\rangle_d+\langle x\rangle_{ds}+2\cdot(n-1)\cdot\langle x\rangle_{sea} = 1\ , \tag{A.6}$$
$$\langle x\rangle_s+\langle x\rangle_{dd}+2\cdot(n-1)\cdot\langle x\rangle_{sea} = 1\ , \tag{A.7}$$

where

$$\langle x\rangle_i=\int_0^1 x\cdot u_i(x)\cdot dx\ , \tag{A.8}$$

and

$$\int_0^1 u_i(x,n)\cdot dx=1,\quad i=q,qq,sea\ . \tag{A.9}$$

For the values $\alpha_R=0.5$, $\alpha_\phi=0$, $\alpha_B=-0.5$, and $k=0$, we obtain $m_1=m_2=\frac{7}{6}(n-1)$.

The fragmentation functions of quarks and diquarks used for the description of strange baryon inclusive spectra are presented here.

For quarks one has:

$$G_s^{\Lambda}(z) = a_{\bar N}\cdot(1-z)^{\lambda+\alpha_R-2\cdot\alpha_B}\cdot(1+a_1z^{a_{1n}})\ , \tag{A.10}$$
$$G_s^{\bar\Lambda}(z) = a_{\bar\Lambda}\cdot(1-z)^{\lambda+\alpha_R-2\alpha_B+2(1-\alpha_R)+2\Delta\alpha}\cdot(1+a_1z^{a_{1n}})\ , \tag{A.11}$$
$$G_u^{\Sigma^+}(z) = G_d^{\Sigma^-}(z)=a_{\bar\Sigma^\pm}\cdot(1-z)^{\lambda+\alpha_R-2\alpha_B+\Delta\alpha}\cdot(1+a_1z^{a_{1n}})\ , \tag{A.12}$$
$$G_u^{\Sigma^-}(z) = G_d^{\Sigma^+}(z)=a_{\bar\Sigma^\pm}\cdot(1-z)^{\lambda+\alpha_R-2\alpha_B+2(1-\alpha_R)+\Delta\alpha}\cdot(1+a_1z^{a_{1n}})\ , \tag{A.13}$$
$$G_s^{\Sigma^-}(z) = G_s^{\Sigma^+}(z)=\frac{a_{\bar\Sigma}}{a_{\bar\Lambda}}\cdot G_s^{\Lambda}(z)\ , \tag{A.14}$$
$$G_s^{\Xi^-}(z) = a_{\overline{\Lambda}}\cdot(1-z)^{\lambda+\alpha_R-2\alpha_B+\Delta\alpha}\cdot(1+a_1z^{a_{1n}})\ , \tag{A.15}$$
$$G_s^{\bar\Xi^+}(z) = a_{\overline{\Xi}}\cdot(1-z)^{\lambda+\alpha_R-2\alpha_B+3\Delta\alpha+2(1-\alpha_R)}\cdot(1+a_1z^{a_{1n}})\ , \tag{A.16}$$
$$G_s^{\Omega}(z) = a_{\overline{\Xi}}\cdot(1-z)^{\lambda+\alpha_R-2\alpha_B+2\Delta\alpha}\cdot(1+a_1z^{a_{1n}})\ , \tag{A.17}$$

where $\Delta\alpha = \alpha_R - \alpha_\phi$, $a_1 = 12$, $a_{1n} = 2$, and $\lambda = 2\alpha' \cdot < p_t^2 >= 0.5$. The fragmentation functions which are not presented here can be found in ref. [20]. The values of the parameters $a_{\bar{\Lambda}}$, $a_{\bar{\Sigma}}$, $a_{\bar{\Xi}}$, and $a_{\bar{\Omega}}$ can be obtained from $a_{\bar{N}}$ through quark combinatorics (see below).

The QGSM diquark fragmentation functions corresponding to antibaryons production through the diagram shown in Fig. 2 are the following:

$$G_{uu}^{\bar{\Lambda}} = G_{ud}^{\bar{\Lambda}} = G_{dd}^{\bar{\Lambda}} = a_{\bar{\Lambda}} \cdot (1-z)^{\lambda+(\alpha_R-2\alpha_B)+2(1-\alpha_B)+\Delta\alpha} , \tag{A.18}$$

$$G_{uu}^{\bar{\Xi}} = G_{ud}^{\bar{\Xi}} = G_{dd}^{\bar{\Xi}} = a_{\bar{\Xi}} \cdot (1-z)^{\Delta\alpha} \cdot G_{uu}^{\bar{\Lambda}} , \tag{A.19}$$

$$G_{ds}^{\bar{\Lambda}} = a_{\bar{\Lambda}} \cdot (1-z)^{\lambda+(\alpha_R-2\alpha_B)+2(1-\alpha_B)+2\Delta\alpha} , \tag{A.20}$$

$$G_{ds}^{\bar{\Xi}} = \frac{a_{\bar{\Xi}}}{a_{\bar{\Lambda}}} \cdot (1-z)^{\Delta\alpha} \cdot G_{ds}^{\bar{\Lambda}} , \tag{A.21}$$

For the diquark fragmentation functions to baryon production, and as it was mentioned in the main text, they have more complicated forms than the quark fragmentation functions, and they contain two different contributions. The first one corresponds to the central production of one $B\bar{B}$ pair, and it is accounted for in Eq. (4) by fragmentation functions with the form:

$$G_{uu}^{\Lambda} = G_{ud}^{\Lambda} = G_{dd}^{\Lambda} = a_{\bar{\Lambda}} \cdot (1-z)^{\lambda-\alpha_R+4(1-\alpha_B)+\Delta\alpha} , \tag{A.22}$$

$$G_{uu}^{\Sigma^+} = G_{dd}^{\Sigma^-} = G_{uu}^{\Sigma^-} = G_{dd}^{\Sigma^+} = G_{ud}^{\Sigma^+} = G_{ud}^{\Sigma^-} = a_{\bar{\Sigma}^\pm} \cdot (1-z)^{\lambda-\alpha_R+4(1-\alpha_B)+\Delta\alpha} , \tag{A.23}$$

$$G_{uu}^{\Xi^-} = G_{ud}^{\Xi^-} = G_{dd}^{\Xi^-} = \frac{a_{\bar{\Xi}}}{a_{\bar{\Lambda}}} \cdot (1-z)^{\Delta\alpha} \cdot G_{uu}^{\Lambda} , \tag{A.24}$$

$$G_{uu}^{\Omega} = G_{ud}^{\Omega} = G_{dd}^{\Omega} = a_{\bar{\Omega}} \cdot (1-z)^{\lambda-\alpha_R+4(1-\alpha_B)+3\Delta\alpha} , \tag{A.25}$$

$$G_{ds}^{\Lambda} = a_{\bar{\Lambda}} \cdot (1-z)^{\lambda-\alpha_R+4(1-\alpha_B)+2\Delta\alpha} , \tag{A.26}$$

$$G_{ds}^{\Sigma^-} = G_{ds}^{\Sigma^+} = \frac{a_{\bar{\Sigma}}}{a_{\bar{\Lambda}}} \cdot G_{ds}^{\Lambda} , \tag{A.27}$$

$$G_{ds}^{\Xi^-} = \frac{a_{\bar{\Xi}}}{a_{\bar{\Lambda}}} \cdot (1-z)^{\Delta\alpha} \cdot G_{ds}^{\Lambda} , \tag{A.28}$$

$$G_{ds}^{\Omega} = \frac{a_{\bar{\Omega}}}{a_{\bar{\Xi}}} \cdot (1-z)^{\lambda-\alpha_R+4(1-\alpha_B)+4\Delta\alpha} . \tag{A.29}$$

In these expressions we have used different parameterizations for the diquark fragmentation functions to antibaryon production and to central baryon production, since antibaryons are produced one cut kink higher in the multiperipheral chain than the companion baryon (see Figure 2). The corresponding expressions for proton and Λ production in pp collision were first given in ref. [2].

The second contribution in the diquark fragmentation functions to baryon production comes from the direct fragmentation of the initial baryon into the secondary one with conservation of SJ, shown in Figs. 3. These contributions are determined by the following fragmentation functions:

$$G_{dd}^{\Lambda} = a_N \cdot z^\beta \cdot \Big[v_0^\Lambda \cdot \varepsilon \cdot (1-z)^2 + v_d^\Lambda \cdot z^{2-\beta} \cdot (1-z)$$

$$
\begin{aligned}
&+ \quad v_{dd}^{\Lambda} \cdot z^{2.5-\beta} \cdot (1-z)\Big] \cdot (1-z)^{\Delta\alpha} \,, && \text{(A.30)}\\
G_{ds}^{\Lambda} &= a_N \cdot z^{\beta} \cdot \Big[v_0^{\Lambda} \cdot \varepsilon \cdot (1-z)^{2+\Delta\alpha} + (v_d^{\Lambda} \cdot z^{2-\beta} \cdot (1-z)^{1+\Delta\alpha} \\
&+ \quad v_s^{\Lambda} \cdot z^{2-\beta+\Delta\alpha} \cdot (1-z)) + v_{ds}^{\Lambda} \cdot z^{2.5-\beta} \cdot (1-\frac{z}{3})\Big] \,, && \text{(A.31)}\\
G_{uu}^{\Sigma^+} &= G_{dd}^{\Sigma^-} = a_N \cdot z^{\beta} \cdot \Big[v_0^{\Sigma^-} \cdot \varepsilon \cdot (1-z)^2 + v_d^{\Sigma^-} \cdot z^{2-\beta} \cdot (1-z) \\
&+ \quad v_{dd}^{\Sigma^-} \cdot z^{2.5-\beta}\Big] \cdot (1-z)^{\Delta\alpha} \,, && \text{(A.32)}\\
G_{ud}^{\Sigma^+} &= G_{ud}^{\Sigma^-} = a_N \cdot z^{\beta} \cdot \Big[v_0^{\Sigma^-} \cdot \varepsilon \cdot (1-z)^2 \\
&+ \quad v_d^{\Sigma^-} \cdot z^{2-\beta} \cdot (1-z)\Big] \cdot (1-z)^{\Delta\alpha} \,, && \text{(A.33)}\\
G_{dd}^{\Sigma^+} &= G_{uu}^{\Sigma^-} = a_N \cdot z^{\beta} \cdot \Big[v_0^{\Sigma^-} \cdot \varepsilon \cdot (1-z)^2\Big] \cdot (1-z)^{\Delta\alpha} \,, && \text{(A.34)}\\
G_{ds}^{\Sigma^+} &= a_N \cdot z^{\beta} \cdot \Big[v_0^{\Sigma^+} \cdot \varepsilon \cdot (1-z)^{2+\Delta\alpha} \\
&+ \quad v_s^{\Sigma^+} \cdot z^{2-\beta} \cdot (1-z)^{1+\Delta\alpha} + v_{ds} \cdot z^{2.5-\beta} \cdot (1-z)\Big] \,, && \text{(A.35)}\\
G_{ds}^{\Sigma^-} &= a_N \cdot z^{\beta} \cdot \Big[v_0^{\Sigma^-} \cdot \varepsilon \cdot (1-z)^{2+\Delta\alpha} + (v_d^{\Sigma^-} \cdot z^{2-\beta} \cdot (1-z)^{1+\Delta\alpha} \\
&+ \quad v_s^{\Sigma^-} \cdot z^{2-\beta+\Delta\alpha} \cdot (1-z)^{1+\Delta\alpha}) + v_{ds} \cdot z^{2.5-\beta}\Big] \,, && \text{(A.36)}\\
G_{dd}^{\Xi^-} &= G_{ud}^{\Xi^-} = a_N \cdot z^{\beta} \cdot [v_0^{\Xi^-} \cdot \varepsilon \cdot (1-z)^2 + v_d^{\Xi^-} \cdot z^{2-\beta} \cdot (1-z)] \cdot (1-z)^{2\Delta\alpha} \,, && \text{(A.37)}\\
G_{ds}^{\Xi^-} &= a_N \cdot z^{\beta} \cdot [v_0^{\Xi^-} \cdot \varepsilon \cdot (1-z)^{2+\Delta\alpha} + v_s^{\Xi^-} \cdot z^{2-\beta} \cdot (1-z)^{1+\Delta\alpha} \\
&+ \quad v_{ds}^{\Xi^-} \cdot z^{2.5-\beta}\Big] \cdot (1-z)^{\Delta\alpha} \,, && \text{(A.38)}\\
G_{uu}^{\Omega^-} &= G_{ud}^{\Omega^-} = G_{dd}^{\Omega^-} = a_N \cdot v_0^{\Omega^-} \cdot \varepsilon \cdot z^{\beta} \cdot (1-z)^{2+3\Delta\alpha} \,, && \text{(A.39)}\\
G_{ds}^{\Omega} &= a_N \cdot z^{\beta} \cdot [v_0 \cdot \varepsilon \cdot (1-z)^{1+2\Delta\alpha} + v_{ds} \cdot z^{2-\beta}] \cdot (1-z)^{1+2\Delta\alpha} \,. && \text{(A.40)}
\end{aligned}
$$

The third term in eqs. (A.30) and (A.31) describes the contribution of the leading resonance Σ^{*-} and its subsequent decay into $\Lambda + \pi$ to the dd and ds fragmentation functions into Λ. The factors $(1-z)$ in Eq. (A.30) and $(1-\frac{z}{3})$ in Eq. (A.31) account for the suppression of this contribution.

The different probabilities for the SJ without valence quarks, v_0^B, the SJ with one valence quark, v_q^B, and the SJ with two valence quarks, v_{qq}^B, to go into the secondary baryon B were deduced through quark combinatorics [26, 27]. Here we assume that the strange quark suppression is common to the three diagrams shown in Fig. 3, and thus, e.g. for the fragmentation of the SJ without valence quarks into different baryons one gets:

$$
p : n : \Lambda + \Sigma : \Xi^0 : \Xi^- : \Omega^- = 4L^3 : 4L^3 : 12L^2S : 3LS^2 : 3LS^2 : S^3 \,, \qquad \text{(A.41)}
$$

where the ratio S/L determines the strange suppression factor, and $2L + S = 1$. In the numerical calculations we have used $S/L = 0.32$.

Following the standard treatment in which the Σ^0 are included into Λ, and to discriminate Λ from the charged Σ, we use the empirical rule: $\Sigma^+ + \Sigma^- = 0.6 \cdot \Lambda$ [27].

The values of v_0^B, v_q^B, and v_{qq}^B used in Eq. (9) are presented in Table 1.

B	p	n	$\Lambda + \Sigma^0$	Σ^+	Σ^-	Ξ^0	Ξ^-	Ω^-
v_0	$4L^3$	$4L^3$	$7.5L^2S$	$(9/4)L^2S$	$(9/4)L^2S$	$3LS^2$	$3LS^2$	S^3
v_u	$3L^2$	L^2	$(5/2)LS$	$(3/2)LS$	-	S^2	-	-
v_d	L^2	$3L^2$	$(5/2)LS$	-	$(3/2)LS$	-	S^2	-
v_s	-	-	$(5/2)L^2$	$(3/4)L^2$	$(3/4)L^2$	$2LS$	$2LS$	S^3
v_{uu}	$2L$	-	$(1/4)S$	$(3/4)S$	-	-	-	-
v_{ud}	L	L	S	-	-	-	-	-
v_{dd}	-	$2L$	$(1/4)S$	-	$(3/4)S$	-	-	-
v_{us}	-	-	$(5/4)L$	$(3/4)L$	-	S	-	-
v_{ds}	-	-	$(5/4)L$	-	$(3/4)L$	-	S	-
v_{ss}	-	-	-	-	-	L	L	S

Table 1: The values of parameters v_i^B in Eq. (9) obtained from quark combinatorics.

Finally, we obtain from Eq. (A.41) the relations among the values of the corresponding parameters $a_{\bar{B}}$ in the fragmentation functions needed in Eq. (4) for the production of different $B\bar{B}$ pairs:

$$\begin{aligned} a_{\bar{N}} : a_{\bar{\Lambda}} : a_{\bar{\Sigma}^\pm} : a_{\bar{\Xi}} : a_{\bar{\Omega}} = 1 \quad &: \quad \sqrt{(15/8)\cdot(S/L)} : \sqrt{(9/16)\cdot(S/L)} : \sqrt{(3/4)\cdot(S/L)^2} \\ &: \quad \sqrt{(3/4)\cdot(S/L)^2} : \sqrt{(1/4)\cdot(S/L)^3}\,. \end{aligned} \tag{A.42}$$

References

[1] A. B. Kaidalov, K. A. Ter–Martirosyan, Yad. Fiz. **39**, 1545 (1984); **40**, 211 (1984).

[2] A. B. Kaidalov, O. I. Piskunova, Yad. Fiz. **41**, 1278 (1985); Z. Phys. **C30**, 145 (1986).

[3] A. Capella, U. Sukhatme, C. I. Tan, J. Tran Thanh Van, Phys. Rep. **236**, 225 (1994).

[4] A. Capella, J. Tran Thanh Van, Z. Phys. C**10**, 249 (1981);
A. Capella, C. Pajares, A. V. Ramallo, Nucl. Phys. **B241**, 75 (1984).

[5] A. B. Kaidalov, K. A. Ter-Martirosyan, Yu. M. Shabelski, Yad. Fiz. **43**, 1282 (1986).

[6] Yu. M. Shabelski, Yad. Fiz. **44**, 186 (1986).

[7] V. A. Abramovsky, V. N. Gribov, O. V. Kancheli, Yad. Fiz. **18**, 595 (1973).

[8] C. Pajares, Yu. M. Shabelski, *Relativistic Nuclear Interactions*, Editorial URSS, Moscow, 2007.

[9] A. B. Kaidalov, Sov. J. Nucl. Phys. **45**, 902 (1987); Yad. Fiz. **45**, 1452 (1987).

[10] M. I. Adamovich et al., WA89 Collaboration, Z. Phys. **C76**, 35 (1997); Eur. Phys. J. **C22**, 255 (2001); Eur. Phys. J. **C26**, 357 (2003).

[11] X. Artru, Nucl. Phys. **B85**, 442 (1975).

[12] M. Imachi, S. Otsuki, F. Toyoda, Prog. Theor. Phys. **52**, 346 (1974); **54**, 280 (1976); **55**, 551 (1976).

[13] G. C. Rossi, G. Veneziano. Nucl. Phys. **B123**, 507 (1977).

[14] G. H. Arakelyan, P. E. Volkovitsky, Z. Phys. **A353**, 87 (1995).

[15] K. A. Ter-Martirosyan, Phys. Lett. **44B**, 377 (1973).

[16] Yu. M. Shabelski, Yad.Fiz. **26**, 1084 (1977); Nucl. Phys. **B132**, 491 (1978).

[17] L. Bertocchi, D. Treleani, J. Phys. **G3**, 147 (1977).

[18] J. Weis, Acta Phys. Polonica **B7**, 85 (1977).

[19] T. Jaroszewicz et al., Z. Phys. **C1**, 181 (1979).

[20] G. H. Arakelyan, A. Capella, A. B. Kaidalov, Yu. M. Shabelski, Eur. Phys. J. **C26**, 81 (2002) and hep-ph/0103337.

[21] F. Bopp, Yu. M. Shabelski, Yad. Fiz. **68**, 2155 (2005) and hep-ph/0406158; Eur. Phys. J. A **28**, 237 (2006) and hep-ph/0603193.

[22] G. H. Arakelyan, C. Merino, Yu. M. Shabelski, Yad. Fiz. **69**, 911 (2006) and hep-ph/0505100; Phys. Atom. Nucl. **70**, 1110 (2007) and hep-ph/0604103; Eur. Phys. J. **A31**, 519 (2007) and hep-ph/0610264; Eur. Phys. J. **C54**, 577 (2008) and hep-ph/0707.1491.

[23] O. I. Piskounova, Phys. Atom. Nucl. **70**, 1110 (2007) and hep-ph/0604157.

[24] Yu. M. Shabelski, hep-ph/0705.0947.

[25] G. H. Arakelyan, C. Merino, C. Pajares, Yu. M. Shabelski, Eur. Phys. J. **C54**, 577 (2008) and hep-ph/0709.3174.

[26] V. V. Anisovich, V. M. Shekhter, Nucl. Phys. **B55**, 455 (1973).

[27] A. Capella, C. A. Salgado, Phys. Rev. **C60**, 054906 (1999).

[28] A.E. Brenner et al., Phys. Rev. **D26**, 1497 (1982).

[29] M. Aguilar-Benítez et al., Z. Phys. **C50**, 405 (1991).

[30] D.S. Barton et al., Phys. Rev. **D27**, 2560 (1983).